JACS
JOURNAL OF THE AMERICAN CHEMICAL SOCIETY
pubs.acs.org/JACS
Article

Organic Laser Molecule with High Mobility, High Photoluminescence Quantum Yield, and Deep-Blue Lasing Characteristics

Dan Liu, Jianbo De, Haikuo Gao, Suqian Ma, Qi Ou, Shuai Li, Zhengsheng Qin, Huanli Dong,* Qing Liao, Bin Xu, Qian Peng, Zhigang Shuai, Wenjing Tian, Hongbing Fu, Xiaotao Zhang, Yonggang Zhen, and Wenping Hu

Cite This: J. Am. Chem. Soc. 2020, 142, 6332−6339

Read Online

ACCESS | Metrics & More | Article Recommendations | Supporting Information

ABSTRACT: Here, we design and synthesize an organic laser molecule, 2,7-diphenyl-9*H*-fluorene (LD-1), which has state-of-the-art integrated optoelectronic properties with a high mobility of 0.25 $cm^2\ V^{-1}\ s^{-1}$, a high photoluminescence quantum yield of 60.3%, and superior deep-blue laser characteristics (low threshold of P_{th} = 71 $\mu J\ cm^{-2}$ and P_{th} = 53 $\mu J\ cm^{-2}$ and high quality factor (Q) of ∼3100 and ∼2700 at emission peaks of 390 and 410 nm, respectively). Organic light-emitting transistors based on LD-1 are for the first time demonstrated with obvious electroluminescent emission and gate tunable features. This work opens the door for a new class of organic semiconductor laser molecules and is critical for deep-blue optical and laser applications.

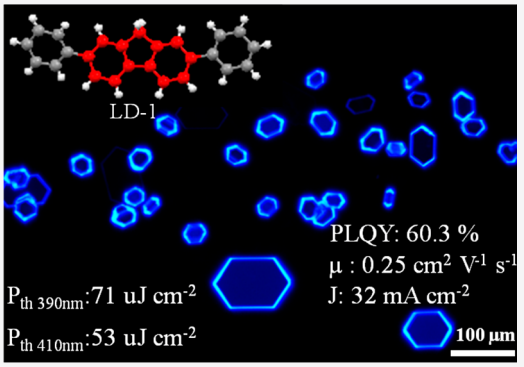

INTRODUCTION

Organic laser semiconducting molecules are the basis of organic light-emitting transistors (OLETs) and electrically pumped organic lasers (EPOLs), which demonstrate great promise for smart display technology, organic lasers, biosensing, and other related optoelectronic circuits.[1−5] However, it remains a big challenge for the development of molecules for OLETs and EPOLs over the past decades.[6−11] One of the key restrictive factors is the design motif integrating high mobility, strong emission for efficient electro-optic conversion, and ideal laser characteristics to achieve a sufficiently high number of excited states under high current density to initiate lasing.[8,9,12,13] Designing highly π-extended fused conjugated systems is one effective approach to increasing charge transport for high mobility;[14−16] however, such kinds of molecules always show very weak fluorescence in the solid state due to the significant quenching of excited states induced by condensed molecular packing and remarkable singlet fissions.[17,18] Reducing the π-conjugation and intermolecular interactions enough may enhance the fluorescence efficiency of organic materials but generally at the cost of efficient charge transport property.[19−21] More recently, achievement of high-mobility emissive organic semiconductors,[22−26] high-efficiency OLETs,[6,7,27,28] and the exciting indication of current-injection lasing from an organic semiconductor[29] have been demonstrated, which brings the hope and passion of scientists from different fields to this field of research. Generally speaking, to date, such materials are still very limited, and only very few of them could meanwhile possess the characteristic of an amplified spontaneous emission (ASE) phenomenon at reasonably low pump intensities, not to mention simultaneously possessing good optical gain for lasing character.[8,9,30−32]

Here, we design and synthesize a fluorene-based organic semiconductor, 2,7-diphenyl-9*H*-fluorene (LD-1) (Figure 1a), with efficient charge transport, strong emission, as well as superior lasing character. The molecule design concept of the LD-1 compound is as follows: (i) fluorene as the unit core is intrinsically a superior building block for organic lasers;[8,31] (ii) it is easy to get derivatives at the 2 and 7 positions for extending π-conjugation and modulating molecular arrangement to enhance the charge transport; (iii) it is also a promising building block for designing blue emitting materials,[33−35] which is particularly important in displays and lasing but difficult to be achieved; (iv) the introduction of a rotational carbon−carbon bond for extending π-conjugation could modulate both optical and electrical properties for their

Received: January 28, 2020
Published: March 18, 2020

https://dx.doi.org/10.1021/jacs.0c00871
J. Am. Chem. Soc. 2020, 142, 6332−6339

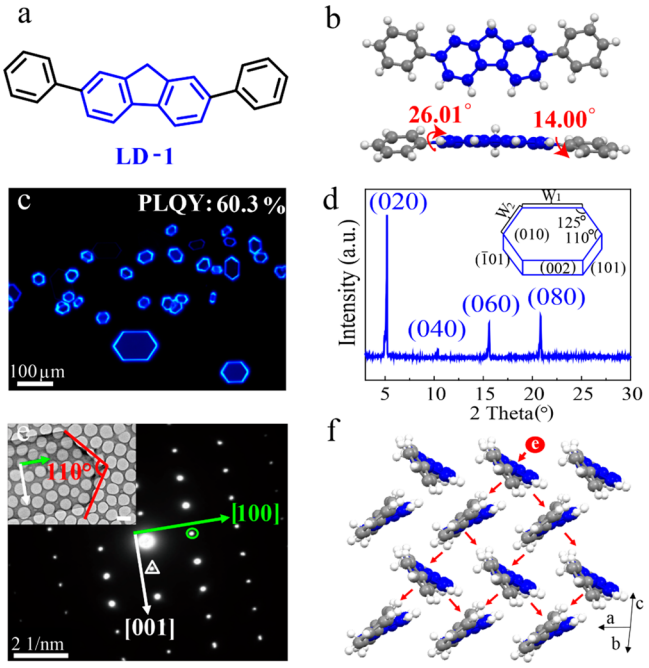

Figure 1. (a) Chemical structure of LD-1 molecule and (b) the views of LD-1 molecule seeing perpendicular (top) to and along (side) the conjugated plane of fluorene core. (c) Fluorescent image of LD-1 single crystals obtained through the PVT technique. (d) XRD patterns of LD-1 single crystals (the inset is a schematic of the elongated hexagon LD-1 crystals with the indexed diffraction planes according to structure analysis). (e) TEM image of an individual crystal and its corresponding SAED pattern. Scale bar: 2 μm. (f) Two-dimensional charge transport routes in LD-1 crystals with herringbone molecular packing.

good integration.[12,22−24,36] Indeed, experimental results demonstrate that the LD-1 compound well integrates the properties of high-mobility charge transport and strong luminescence with a carrier mobility of 0.25 $cm^2\ V^{-1}\ s^{-1}$ and a photoluminescence quantum yield (PLQY) of 60.3% for its single crystals. Moreover, a deep-blue-emissive whispering-gallery-mode (WGM) laser is demonstrated with a low threshold of 71 and 53 $\mu J\ cm^{-2}$ and a high-cavity quality factor (Q) of 3100 and 2700 at emission peaks of 390 and 410 nm, respectively. To our knowledge, LD-1 is among the best performers of deep-blue organic semiconductor lasers integrating efficient charge transport property reported in the literature (Tables S1 and S2). These attractive features of LD-1 make it a good candidate for the research of integrated optoelectronic devices.

RESULTS AND DISCUSSION

LD-1 was synthesized from 2,7-dibromofluorene and phenylboronic acid using a palladium-catalyzed Suzuki coupling reaction with a high yield of 63% (Scheme S1). After the vacuum-sublimation purification process, a milky white powder was obtained. Strong blue emission is easily observed under UV light illumination in both cases of solution and powder, giving a high PLQY of 65 and 50%, respectively (Figure S1). The highest occupied molecular orbital (HOMO) of −5.76 eV was calculated based on the cyclic voltammetry (CV) measurement curve (Figure S2), and the lowest unoccupied molecular orbital (LUMO) of −2.72 eV was further calculated based on the HOMO level and an energy band of 3.04 eV is obtained from its UV−vis curves which will be shown in the following section. Good thermal stability of LD-1 with a sublimation temperature of 337 °C was characterized from thermal gravimetric analysis (TGA) (Figure S3). Large-sized single crystals of LD-1 were obtained via a slow evaporation process from the saturated mixture solution of CH_2Cl_2:ethanol = 1:2 at room temperature. X-ray crystallographic data demonstrates that the LD-1 crystal belongs to an orthorhombic system with cell parameters of a = 5.8687(2) Å, b = 33.6814(8) Å, and c = 8.4453(3) Å (CCDC: 1942276, Table S3). As indicated by single crystal data, a slight rotation angle of 26.01 and 14.00° is determined for the two π-extended benzene rings (left and right) relative to the fluorene core due to the rotation effect of the C−C bond (Figure 1b), which is beneficial for the reduction of the fluorescence quenching effect.[22−24,36] Under the balance of the C−C bond, good electron distributions on the whole molecule at both HOMO and LUMO levels are also demonstrated, which is favorable for forming strong intermolecular interactions to achieve efficient charge transport. A typical herringbone molecular packing mode with a herringbone angle of 64.08° is adopted by LD-1 in single crystals where multiple strong C−H−π interactions (2.730−2.891 Å) between neighboring molecules are formed (Figure S4). All of the results suggest the capacity of LD-1 to integrate strong fluorescence and efficient charge transport properties together.

To further investigate the charge transport and optical property of LD-1, high-quality micro/nanosingle crystals of LD-1 were prepared by physical vapor transport (PVT). Slightly elongated hexagon LD-1 crystals with a side-length (W_1 (long edges)/W_2 (short edges)) ratio centered at around 1.8 based on 100 crystals were usually obtained (Figure S5), which have a smooth surface (root-mean-square (RMS): 0.789 nm) and thickness of around 100 nm characterized by atomic force microscopy (AFM) (Figure S6). A high PLQY of 60.3% was determined for single crystals of LD-1 (Figure 1c), which is slightly lower than that of LD-1 in solution due to the aggregation effect but still maintains the strong emission characteristic, even in a single crystal state. Under 330−380 nm light illumination, a typical optical waveguide feature was observed for LD-1 crystals with a manifestation of very bright emission from their crystal edges suggesting the high quality of the obtained LD-1 crystals, which is a crucial parameter for high optical gain to initiate lasing. Figure 1d shows the X-ray diffraction (XRD) patterns of LD-1 micro/nanocrystals grown on Si/SiO_2 substrate where a series of very sharp and strong diffraction peaks were observed. These diffraction peaks could be well indexed by (0k0) reflections based on single crystal data of LD-1, giving a layer-by-layer growth mode along the b-axis with an interlayer d-spacing of 33.94 Å, indicating that the long axis of the LD-1 molecule is nearly standing on the substrate (Figure S7a). Figure 1e shows the transmission electron microscopy (TEM) image of an individual LD-1 single crystal and its corresponding selected area electron diffraction (SAED) pattern, which was taken by directing the electron beam perpendicular to the flat surface of an individual LD-1 single crystal. The bright and strong multiorder diffraction peaks further confirm the high crystallinity of LD-1 micro/nanocrystals. Based on the LD-1 crystal cell parameters, the spots in the white square and green circle can be ascribed to the Bragg reflections of (001) and (100) planes with $d_{(001)}$ = 8.46 Å and $d_{(100)}$ = 5.93 Å, respectively. Combining XRD and SAED results together, a schematic of

https://dx.doi.org/10.1021/jacs.0c00871
J. Am. Chem. Soc. 2020, 142, 6332−6339

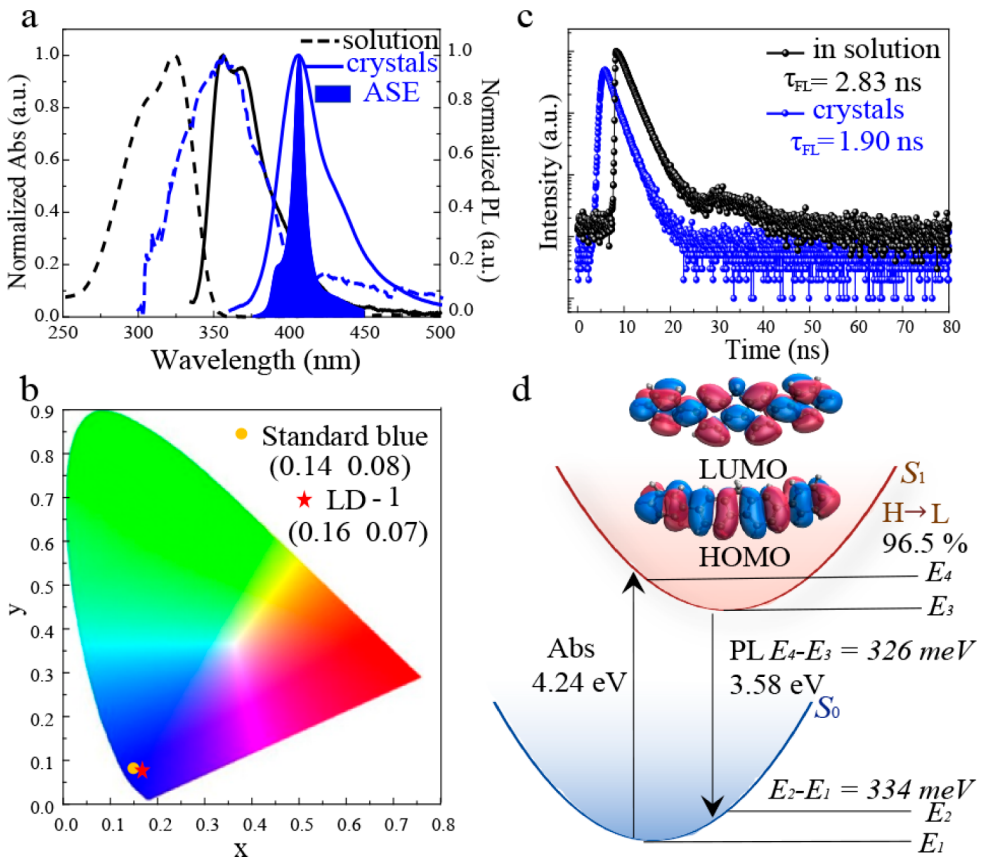

Figure 2. (a) UV−vis absorption, PL, and ASE (filled area) spectra for the LD-1 in CH_2Cl_2 solution and crystals. (b) CIE 1931 coordinates of the LD-1 crystals. (c) Time-resolved peak fluorescence of LD-1 in CH_2Cl_2 solution and crystals. (d) Schematic graph of the four-energy level of LD-1 molecule and the HOMO and LUMO in crystals.

Table 1. Summary of Photophysical Properties of LD-1 in CH_2Cl_2 Solution and Crystals

LD-1	λ_{abs}[a] (nm)	ε_{max}[a] (M^{-1} cm^{-1})	λ_{em}[a] (nm)	Φ_F[a,b]	τ_{FL}[c] (ns)	k_r[d] (s^{-1})	k_{nr}[e] (s^{-1})
in solution	307 323	4.4×10^4	356 368	0.65	2.83	2.30×10^8	1.24×10^8
crystals	353		407	0.60	1.90	3.16×10^8	2.11×10^8

[a]In CH_2Cl_2 solution (1×10^{-5} M). [b]Φ_F of the absolute photoluminescence quantum yield (PLQY) via using the integrating sphere. [c]Fluorescence lifetime. [d]Radiative deactivation rate calculated according to the $k_r = \Phi_F/\tau_{FL}$ equation. [e]Nonradiative deactivation rate calculated according to the $k_{nr} = 1/\tau_{FL} - k_r$ equation.

LD-1 crystal planes in hexagon morphology is shown in the inset of Figure 1d, where the crystals (010) and ($0\bar{1}0$) crystal planes are on the top and bottom bound by (002), ($00\bar{2}$), ($\bar{1}01$), ($10\bar{1}$), (101), and ($\bar{1}0\bar{1}$) crystal planes on the six side-faces, $\angle(00\bar{2})/\angle(10\bar{1}) = 125°$, $\angle(10\bar{1})/\angle(101) = 110°$ (Figure S7b). As shown in Figure 1f, an efficient two-dimensional charge transport network is formed in the direction of *ac* planes, which is parallel to the substrate. In this case, if one molecule gains a charge, it can quickly transfer to the two neighbors and then onto the surrounding molecules, forming a two-dimensional network, which would ensure high mobility in planar organic field-effect transistors (OFETs).[14,37]

The photophysical properties of LD-1 in solution and single crystal state were systematically investigated. Figure 2a shows the UV−vis absorption and photoluminescence (PL) spectra of LD-1 in dichloromethane (CH_2Cl_2) solution and crystals as well as the amplified spontaneous emission (ASE) spectra of LD-1 crystals. Key photophysical parameters measured for LD-1 are summarized in Table 1. A high molar absorption coefficient of 4.4×10^4 M^{-1} cm^{-1} at 323 nm was determined for LD-1 in dilute CH_2Cl_2 solution, a primary parameter ensuring for its strong emission. In comparison with that of solution absorption, an obvious bathochromic shift with the main peaks located at 353 nm is demonstrated for LD-1 crystals, which is one indication of *J*-aggregation in crystals. PL spectra demonstrate that the main emission peak of LD-1 crystal is red-shifted to 407 nm, suggesting LD-1 is a deep-blue emission semiconductor. As we know that, it still remains an urgent task to develop high-performance deep-blue emissive organic semiconductors, though it is greatly crucial in organic optoelectronic devices. According to the National Television Standards Committee (NTSC), the calculated Commission Internationale de l'Éclairage (CIE) coordinates of LD-1 are (0.16, 0.07) (Figure 2b), which are very close to the standard blue CIE coordinates of (0.14, 0.08), suggesting LD-1 is also one of the very few blue emissive organic semiconductors reported so far.[38−40] The superior deep-blue character of LD-1 with CIE $y < 0.10$ suggests its great potential for blue optical and laser applications. The time-resolved fluorescence spectra shown in Figure 2c reveal the reduced fluorescence lifetime (τ) for LD-1 crystals (1.90 ns) compared to that of its CH_2Cl_2 solution (2.83 ns) when fitted by a double-exponential decay

https://dx.doi.org/10.1021/jacs.0c00871
J. Am. Chem. Soc. 2020, 142, 6332−6339

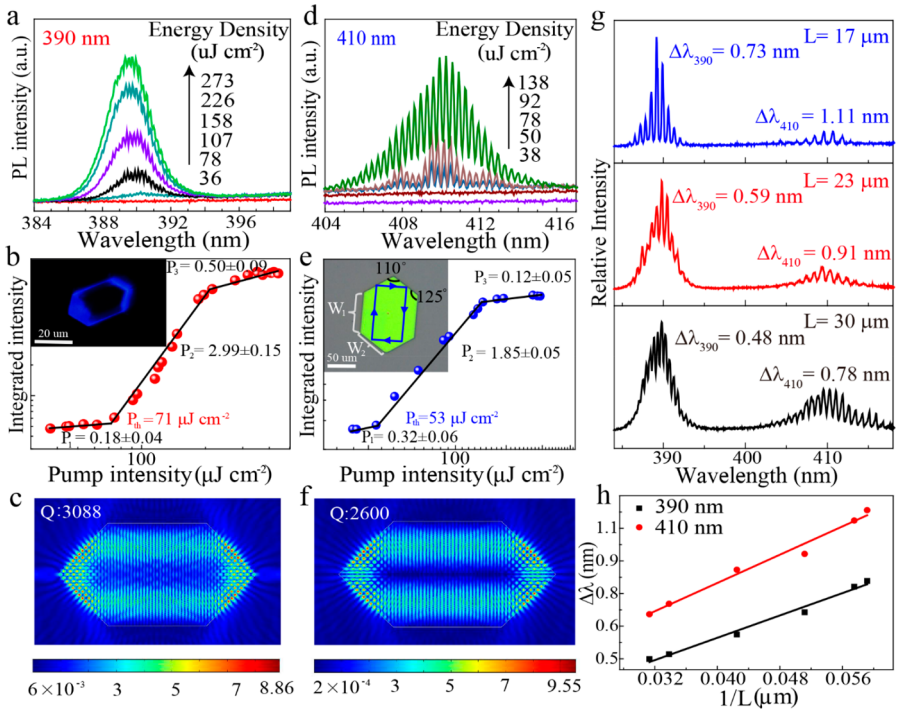

Figure 3. High-resolution PL spectra of the laser emission around 390 nm (a) and 410 nm (d) under different pump densities. (b) Integrated area of the peak 390 nm as a function of pump density. The lasing threshold is identified as the intersection between the sublinear and superlinear regions. Inset: forth bright PL edges of the LD-1 single crystal under 355 nm fs laser excitation. (e) Integrated area of the peak (410 nm) as a function of pump density. Inset: illustrate a typical optical-ray analysis within WGM- LD-1 microcavity. Optical mode simulation results for a LD-1 single crystal with W_1 = 18 μm and W_2 = 9 μm, Q = 3088 of λ = 390 nm (c) and Q = 2600 of λ = 410 nm (f). (g) High-resolution PL spectra of laser emission recorded above the threshold for LD-1 with L = 17, 23, and 30 μm. (h) Mode spacing $\Delta\lambda$ at λ = 390 and 410 nm versus 1/L of the LD-1 crystals, showing a clear linear relationship.

model (Table S4). Correspondingly, fast radiative deactivation rates ($k_r = \Phi_F/\tau_{FL}$) of 3.16 × 10^8 and 2.30 × 10^8 s^{-1} are determined for LD-1 in crystals and solution, respectively, suggesting the efficient emission of LD-1 both in solution and in crystals. Typical ASE property was further characterized for LD-1 single crystals when using a 355 nm pulsed laser as the excitation source along with increase of the pulse energy (Figure 2a and Figure S8). A narrowed bandwidth of PL spectrum with a half-maximum (fwhm) of 9.66 nm was observed for LD-1 crystals, and a sharp ASE peak is located at 407 nm, which is well consistent with that of its PL spectrum. A threshold energy of 168 μJ cm^{-2}, high gain coefficient (48 cm^{-1}), and low loss coefficient (5.29 cm^{-1}) were further characterized based on the deep investigations at the ASE peak (Figure S9). In addition, according to the theoretical calculation (Figure 2d, Figure S10, and Table S5), a well-separated four-energy level is formed between the ground state S_0 and the first excited state S_1. Consisting of 96.6% local transition from the HOMO to the LUMO, S_1 is a highly luminescent state with a calculated transition dipole moment larger than 12 D. After being excited to the S_1 state, the molecule will immediately relax to the lowest vibrational level of S_1 (E_3). Spontaneous and stimulated emission will then take place from E_3 to E_2, followed by another immediate vibrational relaxation process to E_1. This four-energy-level system guarantees that more luminophores populate on the E_3 than E_2. A large Stokes shift is observed in both the spectra and the four-energy-level graph. All of the results demonstrate that LD-1 is a superior deep-blue organic semiconductor with very strong emission, good optical waveguide emission, and ASE property for organic solid-state lasers.

Encouraged by the above results, we further investigated the lasing characteristics of LD-1 crystals (Figure 3). Obviously, two main lasing peaks located at 390 and 410 nm were evolved in the PL spectra along with increasing the pulse density (Figure S11), demonstrating a multimode lasing characteristic, as evidenced by the high-resolution PL spectra shown in Figure 3a and d. As can be seen that the two PL spectra display a broad spontaneous emission at low pump density excitation when the pump density exceeds the threshold (P_{th}) of 71 μJ cm^{-2} at 390 nm and P_{th} = 53 μJ cm^{-2} at 410 nm, respectively (Figure 3b and e), a set of sharp peaks merges on the top of spontaneous emission spectra. In addition, the intensity dependence is fitted according to the power law x^p equation.[41] The latter p = 2.99 ± 0.15 (390 nm) and p = 1.85 ± 0.05 (410 nm) above the threshold were further calculated, indicating a superlinear regime with a typical characteristic of laser emission. As shown in the left inset of Figure 3b, the strong deep-blue laser emission occurs on the top four edges of LD-1 single crystal, indicating that the LD-1 single crystal can act as an efficient 2D microresonator of whispering-gallery-mode (WGM). It could be deduced that the light was totally reflected by the four edges and transported along an oblong route in the crystal, as shown in the inset of Figure 3e. To confirm the WGM microresonator, the dependence of the spacing between adjacent modes ($\Delta\lambda$) on the optical path length (L) of LD-1 single crystals was further characterized (Figure 3g). Clearly, the mode spacing $\Delta\lambda$ gradually decreases and exhibits more and more modes with the increase of the optical path length L. Specifically, $\Delta\lambda_{390}$ = 0.73, 0.59, and 0.48 nm were observed for length L = 17, 23, and 30 μm at an emission peak of 390 nm, and a similar phenomenon was also

https://dx.doi.org/10.1021/jacs.0c00871
J. Am. Chem. Soc. 2020, 142, 6332−6339

Table 2. Key Optoelectronic Properties of the LD-1 Compound in a Single Crystal State

material	λ_{abs} (nm)	λ_{em} (nm)	PLQY	λ_{ASE} (nm)	gain (cm^{-1})	loss (cm^{-1})	P_{th}^{Laser} ($\mu J\ cm^{-2}$)	Q	mobility ($cm^2\ V^{-1}\ s^{-1}$)	V_T (V)	$I_{on/off}$
LD-1	353	407	60.3%	407	48	5.29	71 [390 nm] 53 [410 nm]	3100 [390 nm] 2700 [410 nm]	0.25	6	10^6

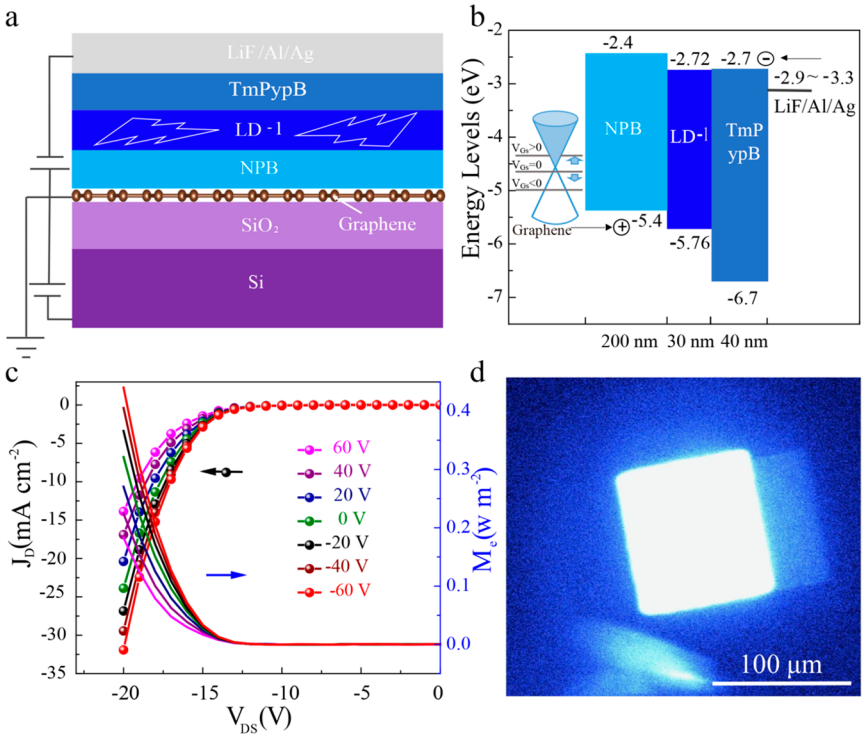

Figure 4. (a) Schematic of the LD-1 based OLET device. (b) Energy level diagram of graphene, NPB, LD-1, and TmPypB and the thickness of each layer used in the device. (c) Typical optical and electrical output characteristics of the LD-1 OLET. (d) The color-coded images of LD-1-OLET extracted from light emission captured by CCD.

observed for the lasing emission peak at 410 nm with $\Delta\lambda_{410}$ = 1.11, 0.91, and 0.78 nm for length L = 17, 23, and 30 μm. Such evolution between $\Delta\lambda$ and length L well corresponds to the characteristic of the WGM cavity.[42,43] To further understand the resonant mode and the relationship of the WGM cavity and mode spacing, the following equation is used

$$\Delta\lambda = \frac{\lambda^2}{L[n - \lambda(dn/d\lambda)]}$$

where $\Delta\lambda$ is the spacing between adjacent modes (Figure S12), $[n - \lambda(dn/d\lambda)]$ is the group refractive index,[42,43] according to geometric conditions, and the optical path length (L) within the resonator could be expressed as

$$L = 2(W_1 + W_2 \times \sin 55^\circ)$$

where W_1 and W_2 are the edge lengths of the LD-1 single crystal (inset image in Figure 1d). The linear increase of $\Delta\lambda$ along with that of increasing $1/L$ further confirms the formation of the WGM-mode cavity for both lasing peaks of 390 and 410 nm (Figure 3h). In addition, the cavity quality factor, another important lasing parameter, is also investigated with the equation of $Q = \lambda/\Delta\lambda_L$, where λ is the lasing peak wavelength and $\Delta\lambda_L$ is the fwhm of the the lasing peak (Figure S12), a significant parameter to evaluate a laser microcavity.[44] Very high experimental Q factors of ~3100 at 390 nm and ~2700 at 410 nm were obtained (Table S6), which are well consistent with those of simulated Q values of 3088 at 390 nm and 2600 at 410 nm (Figure 3c and f). Furthermore, LD-1 single crystals demonstrated good lasing stability during our experimental measurement, which is important for its potential applications.

Furthermore, the charge transport property of LD-1 was investigated based on organic field-effect transistors (Figure S13). Due to the extension of π-conjugation in LD-1 compound ensuring strong intermolecular couplings, efficient electrical transporting property was confirmed for LD-1 with the saturation charge carrier mobility up to 0.25 $cm^2\ V^{-1}\ s^{-1}$ calculated from the typical transfer curves of organic field-effect transistors according to the equation $I_{DS} = (\mu WCi/2L)(V_G - V_T)^2$ (Figure S14) which is more than 1 order of magnitude higher than that previously reported for fluorene-based organic laser semiconductors (Figure S15 and Table S2). The integration of superior optical and electrical transport properties for the LD-1 compound (as summarized in Table 2) ensures its application in an integrated optoelectronic device. As an example, OLET, which is possibly the minimized integrated optoelectronic device and also one of the promising device structures for study of EPOLs, was further investigated. Figure 4a shows the schematic image of the LD-1-based OLET where a vacuum-deposited LD-1 thin film is used as the emitting layer and *N*,*N*′-bis(naphthalen-1-yl)-*N*,*N*′-bis (phenyl)-benzidine (NPB) is the hole injection layer and (3,3′-[5′-[3-(3-pyridinyl)phenyl][1,1′:3′,1″-terphenyl]-3,3″-diyl]-

https://dx.doi.org/10.1021/jacs.0c00871
J. Am. Chem. Soc. 2020, 142, 6332−6339

bispyridine) (TmPypB) is the electron injection layer, respectively. A vertical OLET structure was adopted here with the consideration of its intrinsically short conducting channel for high current density and feasible incorporation of optical configuration and distributed feedback geometry for efficient electroluminescence performance and or initiating lasing.[3,45] Figure 4b shows the energy alignment of NPB, LD-1, TmPypB, and the source electrode of graphene. Due to the tunable Fermi level of graphene and thus the Schottky barrier between bottom graphene and the NPB hole injection layer under negative and positive gate voltages, the OLET device can be operated in the on and off states (Figure S16). Furthermore, using other typical electron transporting materials, 1,3,5-tris(2-*N*-phenylbenzimidazolyl)benzene (TPBi) replaces TmPypB, another device structure of Si/SiO_2/graphene (gate)/NPB/LD-1/TPBi/LiF/Al/Ag was also constructed in the experiment. These two devices demonstrated a similar electroluminescence phenomenon with strong emission. Typical electrical and optical output characteristics of LD-1 OLETs (Figure 4c) demonstrate a clear and consistent correlation between the current density and emitting light output power, suggesting the good tunability of such a device under applied gate voltages. With an applied V_{DS} of −20 V and V_{GS} of −60 V, a current density of around 32 mA cm^{-2} was obtained and strong blue electroluminescence was observed, as shown in Figure 4d with uniform emitting character on the overall active region. The intensity of electroluminescence spectra could be obviously increased along with the increase of negative V_G (Figure S17), which is consistent with that of the PL spectrum of LD-1 thin films (Figure S18) with different relative intensity for emission peaks, probably due to the complex effects induced by different molecular packing structures, the optical resonator effect, and the interface effect in the electrically driven electroluminescent devices. In addition, compared to molecules in solution,[46] LD-1 molecules in the single crystal state show relatively good stability under both electrical field and 355 nm pulse laser, which is important for potential device applications. More deep research works are still needed in the future with the emphasis of constructing the appropriate device geometry with an optimized molecular packing structure, high-quality interface contact, integration of photonic structure, and pumping the devices with an electrical pulse signal.[29,47−51]

CONCLUSIONS

In conclusion, an organic laser molecule, LD-1, was designed and synthesized by introducing phenyl units into the emissive fluorene core via a rotational carbon−carbon bond. Efficient charge transport with a carrier mobility of 0.25 $cm^2 V^{-1} s^{-1}$ and strong solid-state emission with a PLQY of 60.3% are demonstrated. Moreover, its single crystals exhibit a unique ASE phenomenon with outstanding deep-blue laser character of low thresholds of 71 and 53 $\mu J\ cm^{-2}$ and high quality (Q) factor of ∼3100 and ∼2700 at emission peaks of 390 and 410 nm, respectively, by WGM resonator. As an example of LD-1 in integrated optoelectronic device application, OLET based on LD-1 was demonstrated. The importance of this work is that (i) we present a superior organic optoelectronic compound, LD-1, that well simultaneously integrates high charge carrier mobility, strong photoluminescence, excellent lasing character, as well as rare and commendable deep-blue optical property; (ii) it opens a door for further developing a series of more efficient organic laser semiconductors toward compact, low-cost display, and laser technology. More systematic research works are ongoing, and we believe much higher performances would be expected in the future by further rational molecular design and device optimization.

ASSOCIATED CONTENT

Supporting Information

The Supporting Information is available free of charge at https://pubs.acs.org/doi/10.1021/jacs.0c00871.

Experimental details, synthesis, characterization, device fabrication, and theoretical studies (CIF)

AUTHOR INFORMATION

Corresponding Author

Huanli Dong − *Beijing National Laboratory for Molecular Science, Key Laboratory of Organic Solids, Institute of Chemistry, Chinese Academy of Sciences, Beijing 100190, China; University of Chinese Academy of Sciences, Beijing 100049, China;* orcid.org/0000-0002-5698-5369; Email: dhl522@iccas.ac.cn

Authors

Dan Liu − *Beijing National Laboratory for Molecular Science, Key Laboratory of Organic Solids, Institute of Chemistry, Chinese Academy of Sciences, Beijing 100190, China; University of Chinese Academy of Sciences, Beijing 100049, China*

Jianbo De − *Beijing Key Laboratory for Optical Materials and Photonic Devices, Department of Chemistry, Capital Normal University, Beijing 100048, China*

Haikuo Gao − *Beijing National Laboratory for Molecular Science, Key Laboratory of Organic Solids, Institute of Chemistry, Chinese Academy of Sciences, Beijing 100190, China; University of Chinese Academy of Sciences, Beijing 100049, China*

Suqian Ma − *State Key Laboratory of Supramolecular Structure and Materials, Jilin University, Changchun 130012, China*

Qi Ou − *Department of Chemistry, Tsinghua University, Beijing 100084, China*

Shuai Li − *Beijing Key Laboratory for Optical Materials and Photonic Devices, Department of Chemistry, Capital Normal University, Beijing 100048, China*

Zhengsheng Qin − *Beijing National Laboratory for Molecular Science, Key Laboratory of Organic Solids, Institute of Chemistry, Chinese Academy of Sciences, Beijing 100190, China; University of Chinese Academy of Sciences, Beijing 100049, China*

Qing Liao − *Beijing Key Laboratory for Optical Materials and Photonic Devices, Department of Chemistry, Capital Normal University, Beijing 100048, China*

Bin Xu − *State Key Laboratory of Supramolecular Structure and Materials, Jilin University, Changchun 130012, China;* orcid.org/0000-0002-0423-925X

Qian Peng − *Beijing National Laboratory for Molecular Science, Key Laboratory of Organic Solids, Institute of Chemistry, Chinese Academy of Sciences, Beijing 100190, China;* orcid.org/0000-0001-8975-8413

Zhigang Shuai − *Department of Chemistry, Tsinghua University, Beijing 100084, China;* orcid.org/0000-0003-3867-2331

Wenjing Tian − *State Key Laboratory of Supramolecular Structure and Materials, Jilin University, Changchun 130012, China;* orcid.org/0000-0001-5766-8050

https://dx.doi.org/10.1021/jacs.0c00871
J. Am. Chem. Soc. 2020, 142, 6332−6339

Hongbing Fu − *Beijing Key Laboratory for Optical Materials and Photonic Devices, Department of Chemistry, Capital Normal University, Beijing 100048, China;* orcid.org/0000-0003-4528-189X

Xiaotao Zhang − *Tianjin Key Laboratory of Molecular Optoelectronic Sciences, Department of Chemistry, School of Science, Tianjin University and Collaborative Innovation Center of Chemical Science and Engineering, Tianjin 300072, China;* orcid.org/0000-0002-0123-025X

Yonggang Zhen − *Beijing National Laboratory for Molecular Science, Key Laboratory of Organic Solids, Institute of Chemistry, Chinese Academy of Sciences, Beijing 100190, China;* orcid.org/0000-0003-4506-4449

Wenping Hu − *Tianjin Key Laboratory of Molecular Optoelectronic Sciences, Department of Chemistry, School of Science, Tianjin University and Collaborative Innovation Center of Chemical Science and Engineering, Tianjin 300072, China;* orcid.org/0000-0001-5686-2740

Complete contact information is available at: https://pubs.acs.org/10.1021/jacs.0c00871

Notes

The authors declare no competing financial interest.

■ ACKNOWLEDGMENTS

The authors acknowledge the financial support from the Ministry of Science and Technology of China (2017YFA0204503, 2018YFA0703200, 2016YFB0401100), the National Natural Science Foundation of China (51725304, 61890943, 91833306, 51733004, 21875259, 51633006), Beijing National Laboratory for Molecular Sciences (BNLMS-CXXM-202012), the Youth Innovation Promotion Association of the Chinese Academy of Sciences, and the National Program for Support of Top-notch Young Professionals.

■ REFERENCES

(1) Muccini, M.; Toffanin, S. *Organic light-emitting transistors: towards the next generation display technology*; Wiley-Science Wise Co-Publication: Hoboken, NJ, 2016.
(2) Muccini, M. A bright future for organic field-effect transistors. *Nat. Mater.* **2006**, *5*, 605−613.
(3) McCarthy, M. A.; Liu, B.; Donoghue, E. P.; Kravchenko, I.; Kim, D. Y.; So, F.; Rinzle, A. G. Low-voltage, low-power, organic light-emitting transistors for active matrix Displays. *Science* **2011**, *332*, 570−573.
(4) Capelli, R.; Toffanin, S.; Generali, G.; Usta, H.; Facchetti, A.; Muccini, M. Organic light-emitting transistors with an efficiency that outperforms the equivalent light-emitting diodes. *Nat. Mater.* **2010**, *9*, 496−503.
(5) Hou, L. L.; Zhang, X. Y.; Cotella, G. F.; Carnicella, G.; Herder, M.; Schmidt, B. M.; Pätzel, M.; Hecht, S.; Cacialli, F.; Samorì, P. Optically switchable organic light-emitting transistors. *Nat. Nanotechnol.* **2019**, *14*, 347−353.
(6) Zhang, C.; Chen, P.; Hu, W. Organic light-emitting transistors: materials, device configurations, and operations. *Small* **2016**, *12*, 1252−1294.
(7) Liu, C. F.; Liu, X.; Lai, W. Y.; Huang, W. Organic light-emitting field-effect transistors: device geometries and fabrication techniques. *Adv. Mater.* **2018**, *30*, 1802466.
(8) Samuel, I. D. W.; Turnbull, G. A. Organic semiconductor lasers. *Chem. Rev.* **2007**, *107*, 1272−1295.
(9) Tessler, N. Lasers based on semiconducting organic materials. *Adv. Mater.* **1999**, *11*, 363−370.
(10) Bradley, D. D. C. Organic electronics and photonics: concluding remarks. *Faraday Discuss.* **2014**, *174*, 429−438.
(11) Lin, J.; Hu, Y.; Lv, Y.; Guo, X.; Liu, X. Light gain amplification in microcavity organic semiconductor laser diodes under electrical pumping. *Sci. Bull.* **2017**, *62*, 1637−1638.
(12) Zhang, X.; Dong, H.; Hu, W. Organic semiconductor single crystals for electronics and photonics. *Adv. Mater.* **2018**, *30*, 1801048.
(13) Ma, Y. G.; Shen, J. C. Research progress of photoelectric functional organic crystals. *Sci. China, Ser. B* **2007**, *37*, 105−123.
(14) Dong, H.; Fu, X.; Liu, J.; Wang, Z.; Hu, W. 25th Anniversary article: key points for high-mobility organic field-effect transistors. *Adv. Mater.* **2013**, *25*, 6158−6183.
(15) Wadsworth, A.; Chen, H.; Thorley, K. J.; Cendra, C.; Nikolka, M.; Bristow, H.; Moser, M.; Salleo, A.; Anthopoulos, T. D.; Sirringhaus, H.; McCulloch, I. Modification of indacenodithiophene-based polymers and its impact on charge carrier mobility in organic thin-film transistors. *J. Am. Chem. Soc.* **2020**, *142*, 652−664.
(16) Ni, Z. J.; Wang, H. L.; Dong, H. L.; Dang, Y. F.; Zhao, Q.; Zhang, X. T.; Hu, W. P. Mesopolymer synthesis by ligand-modulated direct arylation polycondensation towards n-type and ambipolar conjugated systems. *Nat. Chem.* **2019**, *11*, 271−277.
(17) Anthony, J. E.; Brooks, J. S.; Eaton, D. L.; Parkin, S. R. Functionalized pentacene: improved electronic properties from control of solid-state order. *J. Am. Chem. Soc.* **2001**, *123*, 9482−9483.
(18) Zimmerman, P. M.; Bell, F.; Casanova, D.; Head-Gordon, M. Mechanism for singlet fission in pentacene and tetracene: from single exciton to two triplets. *J. Am. Chem. Soc.* **2011**, *133*, 19944−19952.
(19) Grimsdale, A. C.; Chan, K. L.; Martin, R. E.; Jokisz, P. G.; Holmes, A. B. Synthesis of light-emitting conjugated polymers for applications in electroluminescent devices. *Chem. Rev.* **2009**, *109*, 897−1091.
(20) Huang, Y. J.; Wang, Z. R.; Chen, Z.; Zhang, Q. C. Organic cocrystals: beyond electrical conductivities and field-effect transistors (FETs). *Angew. Chem., Int. Ed.* **2019**, *58*, 9696−9711.
(21) Mei, J.; Leung, N. L. C.; Kwok, R. T. K.; Lam, J. W. Y.; Tang, B. Z. Aggregation-induced emission: together we shine, united we soar. *Chem. Rev.* **2015**, *115*, 11718−11940.
(22) Liu, J.; Zhang, H.; Dong, H.; Meng, L.; Jiang, L.; Jiang, L.; Wang, Y.; Yu, J.; Sun, Y.; Hu, W.; Heeger, A. J. High mobility emissive organic semiconductor. *Nat. Commun.* **2015**, *6*, 10032.
(23) Li, J.; Zhou, K.; Liu, J.; Zhen, Y.; Liu, L.; Zhang, J.; Dong, H.; Zhang, X.; Jiang, L.; Hu, W. Aromatic extension at 2,6-positions of anthracene toward an elegant strategy for organic semiconductors with efficient charge transport and strong solid state emission. *J. Am. Chem. Soc.* **2017**, *139*, 17261−17264.
(24) Chen, M.; Zhao, Y.; Yan, L.; Yang, S.; Zhu, Y.; Murtaza, I.; He, G.; Meng, H.; Huang, W. A unique blend of 2-Fluorenyl-2-anthracene and 2-Anthryl-2anthracence showing white emission and high charge mobility. *Angew. Chem., Int. Ed.* **2017**, *56*, 722−727.
(25) Liu, D.; Li, J.; Liu, J.; Lu, X.; Hu, M.; Li, Y.; Shu, Z.; Ni, Z.; Ding, S.; Jiang, L.; Zhen, Y.; Zhang, X.; Dong, H.; Hu, W. A new organic compound of 2-(2,2-diphenylethenyl)anthracene (DPEA) showing simultaneous electrical charge transport property and AIE optical characteristics. *J. Mater. Chem. C* **2018**, *6*, 3856−3860.
(26) Deng, J.; Xu, Y.; Liu, L.; Feng, C.; Tang, J.; Gao, Y.; Wang, Y.; Yang, B.; Lu, P.; Yang, W.; Ma, Y. An ambipolar organic field-effect transistor based on an AIE-active single crystal with a high mobility level of 2.0 $cm^2 V^{-1} s^{-1}$. *Chem. Commun.* **2016**, *52*, 2370−2373.
(27) Qin, Z. S.; Gao, H. K.; Liu, J.; Zhou, K.; Li, J.; Dang, Y. Y.; Huang, L.; Deng, H. X.; Zhang, X. T.; Dong, H. L.; Hu, W. P. High-efficiency single-component organic light-emitting transistors. *Adv. Mater.* **2019**, *31*, 1903175.
(28) Oh, S.; Kim, J. H.; Park, S. K.; Ryoo, C. H.; Park, S. Y. Fabrication of Pixelated Organic light-emitting transistor (OLET) with a pure red-emitting organic semiconductor. *Adv. Opt. Mater.* **2019**, *7*, 1901274.
(29) Sandanayaka, A. S. D.; Matsushima, T.; Bencheikh, F.; Terakawa, S.; Potscavage, W. J.; Qin, C.; Fujihara, T.; Goushi, K.;

Ribierre, J.-C.; Adachi, C. Indication of current-injection lasing from an organic semiconductor. *Appl. Phys. Express* **2019**, *12*, 061010.
(30) Wang, K.; Gao, Z. H.; Zhang, W.; Yan, Y. L.; Song, H. W.; Lin, X. Q.; Zhou, Z. H.; Meng, H. B.; Xia, A. D.; Yao, J. N.; Zhao, Y. S. Exciton funneling in light-harvesting organic semiconductor microcrystals for wavelength-tunable lasers. *Sci. Adv.* **2019**, *5*, No. eaaw2953.
(31) Yap, B. K.; Xia, R.; Campoy-Quiles, M.; Stavrinou, P. N.; Bradley, D. D. C. Simultaneous optimization of charge-carrier mobility and optical gain in semiconducting polymer films. *Nat. Mater.* **2008**, *7*, 376−380.
(32) Ma, S.; Zhou, K.; Hu, M.; Li, Q.; Liu, Y.; Zhang, H.; Jing, J.; Dong, H.; Xu, B.; Hu, W.; Tian, W. Integrating efficient optical gain in high-mobility organic semiconductors for multifunctional optoelectronic applications. *Adv. Funct. Mater.* **2018**, *28*, 1802454.
(33) Wei, Q.; Li, Y.; Liu, J.; Fang, Q.; Li, J.; Yan, X.; Xie, L.; Qian, Y.; Xia, R.; Huang, W. A high performance deep blue organic laser gain material. *Adv. Opt. Mater.* **2017**, *5*, 1601003.
(34) Qian, Y.; Wei, Q.; Del Pozo, G.; Mroz, M. M.; Lueer, L.; Casado, S.; Cabanillas-Gonzalez, J.; Zhang, Q.; Xie, L.; Xia, R.; Huang, W. H-Shaped oligofluorenes for highly air-stable and low-threshold non-doped deep blue lasing. *Adv. Mater.* **2014**, *26*, 2937−2942.
(35) Schneider, D.; Rabe, T.; Riedl, T.; Dobbertin, T.; Werner, O.; Kroger, M.; Becker, E.; Johannes, H. H.; Kowalsky, W.; Weimann, T.; Becker, J.; Hinze, P.; Gerhard, A.; Stossel, P.; Vestweber, H. Deep blue widely tunable organic solid-state laser based on a spirobifluorene derivative. *Appl. Phys. Lett.* **2004**, *84*, 4693−4695.
(36) Xie, Z. Y.; Liu, D.; Zhang, Y. H.; Liu, Q. Q.; Dong, H. L.; Hu, W. P. Recent advances on high mobility emissive anthracene-derived organic semiconductors. *Chem. Res. Chin. Univ.* **2020**, accepted for publication.
(37) Wang, L.; Nan, G.; Yang, X.; Peng, Q.; Li, Q.; Shuai, Z. Computational methods for design of organic materials with high charge mobility. *Chem. Soc. Rev.* **2010**, *39*, 423−434.
(38) Xing, X.; Zhang, L.; Liu, R.; Li, S.; Qu, B.; Chen, Z.; Sun, W.; Xiao, L.; Gong, Q. A deep-blue emitter with electron transporting Property to improve charge balance for organic light-emitting device. *ACS Appl. Mater. Interfaces* **2012**, *4*, 2877−2880.
(39) Kim, Y. H.; Shin, D. C.; Kim, S. H.; Ko, C. H.; Yu, H. S.; Chae, Y. S.; Kwon, S. K. Novel blue emitting material with high color purity. *Adv. Mater.* **2001**, *13*, 1690−1693.
(40) Gao, Z.; Li, Z.; Xia, P.; Wong, M.; Cheah, K. W.; Chen, C. H. Efficient deep-blue organic light-emitting diodes: arylamine-substituted oligofluorenes. *Adv. Funct. Mater.* **2007**, *17*, 3194−3199.
(41) Kena-Cohen, S.; Forrest, S. R. Room-temperature polariton lasing in an organic single-crystal microcavity. *Nat. Photonics* **2010**, *4*, 371−375.
(42) Wang, X.; Liao, Q.; Kong, Q.; Zhang, Y.; Xu, Z.; Lu, X.; Fu, H. Whispering-gallery-mode microlaser based on self-assembled organic single-crystalline hexagonal microdisks. *Angew. Chem., Int. Ed.* **2014**, *53*, 5863−5867.
(43) Yu, Z.; Wu, Y.; Liao, Q.; Zhang, H.; Bai, S.; Li, H.; Xu, Z.; Sun, C.; Wang, X.; Yao, J.; Fu, H. Self-assembled microdisk lasers of perylenediimides. *J. Am. Chem. Soc.* **2015**, *137*, 15105−15111.
(44) Wang, X.; Li, H.; Wu, Y.; Xu, Z.; Fu, H. Tunable morphology of the self-assembled organic microcrystals for the efficient laser optical resonator by molecular modulation. *J. Am. Chem. Soc.* **2014**, *136*, 16602−16608.
(45) Ma, L.; Yang, Y. Unique architecture and concept for high performance organic transistors. *Appl. Phys. Lett.* **2004**, *85*, 5084−5086.
(46) Kobin, B.; Behren, S.; Braun-Cula, B.; Hecht, S. Photochemical degradation of various bridge-substituted fluorene based materials. *J. Phys. Chem. A* **2016**, *120*, 5474−5480.
(47) Samuel, D. W.; Namdas, E. B.; Turnbull, G. A. How to recognize lasing. *Nat. Photonics* **2009**, *3*, 546−549.
(48) Gwinner, M. C.; Khodabakhsh, S.; Song, M. H.; Schweizer, H.; Giessen, H.; Sirringhaus, H. Integration of a rib waveguide distributed feedback structure into a light-emitting polymer field-effect transistor. *Adv. Funct. Mater.* **2009**, *19*, 1360−1370.
(49) Namdas, E. B.; Tong, M.; Ledochowitsch, P.; Mednick, S. R.; Yuen, J. D.; Moses, D.; Heeger, A. J. Low thresholds in polymer lasers on conductive substrates by distributed feedback nanoimprinting: progress toward electrically pumped plastic lasers. *Adv. Mater.* **2009**, *21*, 799−802.
(50) Bisri, S. Z.; Takenobu, T.; Sawabe, K.; Tsuda, S.; Yomogida, Y.; Yamao, T.; Hotta, S.; Adachi, C.; Iwasa, Y. p-i-n homojunction in organic light-emitting transistors. *Adv. Mater.* **2011**, *23*, 2753−2758.
(51) Hotta, S. Optically and electrically excited emissions from organic semiconducting oligomer crystals. *Polym. Int.* **2017**, *66*, 223−236.

https://dx.doi.org/10.1021/jacs.0c00871
J. Am. Chem. Soc. 2020, 142, 6332−6339